Received: 9 December 2020 | Revised: 27 May 2021 | Accepted: 30 May 2021

DOI: 10.1002/jbio.202000486

FULL ARTICLE

JOURNAL OF BIOPHOTONICS

Effect of the presence of amniotic fluid for optical transabdominal fetal monitoring using Monte Carlo simulations

Jacqueline Gunther[1*] | **Baptiste Jayet**[1] | **Adam Jacobs**[2] | **Ray Burke**[1] | **Jana M. Kainerstorfer**[3] | **Stefan Andersson-Engels**[1,4]

[1]Biophotonics@Tyndall, IPIC, Tyndall National Institute, Cork, Ireland

[2]Sunrise Labs, Inc., Bedford, New Hampshire, USA

[3]Department of Biomedical Engineering, Carnegie Mellon University, Pittsburgh, Pennsylvania, USA

[4]Department of Physics, University College Cork, Cork, Ireland

***Correspondence**
Jacqueline Gunther, Biophotonics@Tyndall, IPIC, Tyndall, National Institute, Cork, Ireland.
Email: jacqueline.gunther@tyndall.ie

Funding information
Science Foundation Ireland, Grant/Award Numbers: SFI/12RC/2276 P2, SFI/15RP/2828

Abstract

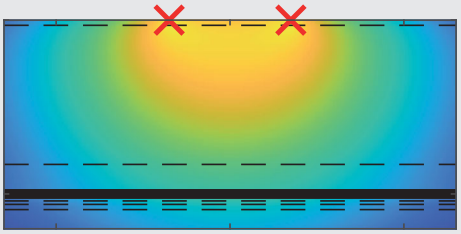

About a third of babies are delivered by Cesarean section. There has been an increase in maternal deaths during labor due to complications with subsequent births after a C-section. Therefore, there is a clinical motivation to reduce the C-section rate. Current techniques are, however, inefficient at determining fetal distress leading to a high false positive rate for complications and ultimately a C-section. For the current study, Monte Carlo simulations were used to calculate the amount of signal received on a model of a pregnant mother, as well as, the percent of the signal that comes from the fetal layer. Models with and without a 1 mm amniotic fluid were compared and showed differing trends.

KEYWORDS

fetal pulse oximetry, light propagation modeling, Monte Carlo, transabdominal fetal monitoring

1 | INTRODUCTION

In 2019, within the United States, delivery by Cesarean section (C-section) represented 31.7% of all births with 25.6% of the cesarean deliveries being low-risk deliveries (first time birth with at least 37 weeks completed with one fetus and head first birth) [1]. The World Health Organization cautions against high C-sections rates stating that rates above 10% do not reduce maternal or newborn mortality rates [2]. There has also been evidence to show that there is a higher risk of maternal death after a C-section due to complications [3]. Current methods of electronic fetal heart rate monitoring are inefficient at determining hypoxia and acidosis in the fetus, which would be valid reasons to perform a surgical delivery. Electronic fetal heart rate monitors lead to false positives of fetal distress detection leading to a higher C-section rate [4]. Therefore, there is a clinical need to develop better fetal monitoring procedures in order to decrease this rate and prevent maternal mortality. Fetal pulse oximetry has the ability to help assess fetal distress accurately. This could help decrease the rate of unnecessary C-sections and maternal deaths by providing clinicians with a tool to help them make the decision when to intervene and

Abbreviations: MC, Monte Carlo.

perform the C-section or when to let the labor to continue naturally.

There are several approaches taken to determine feasibility of fetal pulse oximetry. Computational modeling in the literature [5–14] was used to determine design parameters and efficacy of detection and phantom studies [7, 8, 11, 15–19] were used to test prototypes. Pre-clinical [20–23] and clinical studies [7, 24–28] were performed to determine overall feasibility with the realistic conditions that transabdominal fetal pulse oximetry might encounter.

While there has been a significant amount of effort to determine fetal oxygen using transabdominal pulse oximetry, there is still a clinical need to develop one that works efficiently [29]. We present here Monte Carlo (MC) computational models using commonly and publicly available software without modifications to accurately determine fetal signal. We present here a fetal model to answer the questions: (a) How much light signal can be obtained when the source power is within the safety limits for laser exposure to skin? (b) How does the presence of amniotic fluid affect the signal? (c) How much light signal comes from the fetus and is emitted from the surface of the mother? and (d) How can photon hitting density maps be used to evaluate how much light reaches the fetus? To answer the last two questions, we look at the fetal signal (light that has passed through the fetal layers) and mother only component of the signal compared to the overall signals. We look at the amount of light that reaches the fetus. In traditional pulse oximetry, however, the change in the optical signal due to the pulse from the heart beat is used to determine the arterial oxygen saturation.

MC simulations were used to determine the light signals. The MC model is eight layers including a non-diffuse amniotic layer and was run with 1 billion photon packages for sufficient accuracy. The amniotic fluid layer in the model was removed to observe the effect on the reflection measurement. We examine the photon hitting density maps of several source-detector distances to quantify the probability of light reaching the fetal layer of the model. We also compare the signal levels when amniotic fluid was present or not. There are two reasons to study amniotic fluid layer. First, during pregnancy the width of the amniotic fluid layer will change as the fetus grows, so pre-natal screening may be different from labor monitoring. Second, diffuse optical imaging and diffuse optical modeling are not able to simulate amniotic fluid because of its low scattering properties. Therefore, if diffuse methods are used, it is important to understand the limitations of removing the amniotic fluid layer from potential models. Last, we focus on an illumination power, that is, within the safety standards for lasers.

2 | METHODS

Computational modeling was used to simulate the problem of light propagation through the abdomen of a pregnant woman, who is in the late gestational stages in which the fetal head would make contact with the mother's uterus. The simulation method was a MC-based algorithm (CUDAMCML [30]) which is a GPU based algorithm modified from the widely used MCML algorithm [31]. For this model, taken from ref [13], the abdomen of the pregnant woman and fetus is divided into eight layers with different optical properties that can be found in Table 1. There was one set of simulations done with the amnitotic fluid layer and another set with no amniotic fluid layer. In order to keep the fetal depth the same, 1 mm was added to the maternal subdermal layer. For each layer the anisotropy factor (g) was 0.9. There was a boundary mismatch at the surface with the outside medium considered having an index of refraction of one. The arterial layer of the fetus was not pulsatile in this model but was the expected location of where the pulsatile signal would be found. For this study, we wanted to know how much light actually reaches the fetus. Signals were computed at two different wavelengths (735 and 850 nm) as listed in Table 1 and for seven different fetal depths (20-50 mm at 5 mm increments). The maternal subdermal layer was varied to obtain the range of fetal depths. Since the intensity limitation for skin exposure to near-infrared continuous wave lasers is 200 m W cm^{-2} [32], the values of the power on detector given in the result section assume a source intensity of 200 m W cm^{-2}.

2.1 | MC simulations

The CUDAMCML algorithm works by simulating geometries with radial symmetry, such as a semi-infinite plane or a stack of horizontal layers. A representation of the model that was used is shown in Figure 1. In addition, as CUDAMCML is a GPU-based algorithm, it enables to simulate a large number of photon packages in a reasonable amount of time, therefore each simulation was run using 1 billion photon packages ($\approx$ 1 hour). Since a large number of photon packages were needed to obtain data at far source-detector distances (>8 cm), CUDAMCML was utilized instead of mesh based MC methods, which would take a significant amount of time to run with this many photon packages. The source had a 1 cm^2 circle area by using a convolution technique [35] with a top-hat beam profile. In order to estimate the diffuse reflectance, the detector area was set to 1 cm^2 circle. The MC simulations were converted to Cartesian coordinates from radial coordinates in order to

TABLE 1 Optical properties of the different layers used for Monte Carlo simulations [13]

	735 nm		850 nm			
Layer	μ_a (cm^{-1})	μ_s (cm^{-1})	μ_a (cm^{-1})	μ_s (cm^{-1})	**Index of refraction (n)**	**Width (cm)**
Maternal dermal	0.170	230	0.125	177	1.40	0.15
Maternal subdermal	0.085	120	0.088	111	1.40	0.9–4.0
Maternal uterus	0.160	108	0.100	81.5	1.40	0.85
Amniotic fluid	0.125	1.00	0.042	1.00	1.33	0.10
Fetal scalp	0.157	68.1	0.157	62.3	1.30	0.20
Fetal skull [33, 34]	0.175	350	0.155	300	1.30	0.10
Fetal arterial	0.210	109	0.215	91.0	1.30	0.15
Fetal brain	0.187	122	0.132	98.0	1.30	Semi-infinite

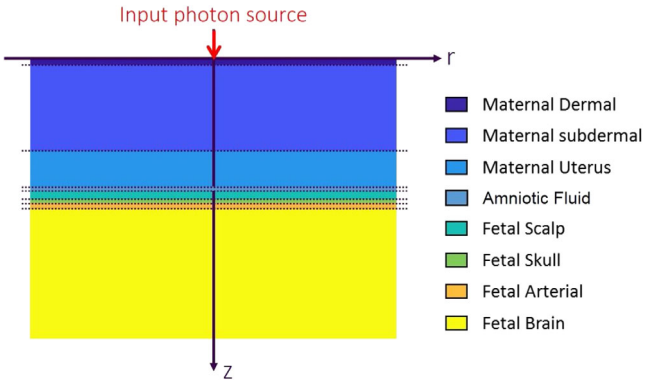

FIGURE 1 Layered model used for Monte Carlo simulation

find the area of the detector. The source-detector distances (0.5-11 cm) were setup in 0.5 cm intervals.

2.2 | Photon hitting density maps

Photon hitting density maps (PHD) were created to understand the depth reached by the photons that have been detected given a fixed source-detector configurations. The maps can be calculated by multiplying the fluence map ($\phi_s\left(\overleftarrow{r}\right)$) of a given source locations with the fluence map ($\phi_d\left(\overleftarrow{r}\right)$) of a field created by a source at a second position, which is the same position as the detector.

$$\mathrm{PHD}\left(\overleftarrow{r}\right) = \phi_s\left(\overleftarrow{r}\right) \times \phi_d\left(\overleftarrow{r}\right), \tag{1}$$

2.3 | Signal from fetus

In order to estimate the detected intensity of light passing through the fetus, two sets of simulations were run in the same geometry but for different tissue properties (see Figure 2). First a set of simulations was run using the normal model with the real optical properties as given by Table 1 and with varying fetal depths. This gives the signal on the detector of a particular source-detector distance, $I_{\mathrm{both}}(d)$. Second, the absorption coefficient of the fetus layers was changed to 10^6 cm^{-1}. In that case, the calculated signal on the detector, $I_{\mathrm{mother}}(d)$, was considered to be consisting of the light that traveled through only the mother layers without entering the fetus layers, since all the light that reached the fetus got absorbed [5]. Then, the intensity of the light that went through the fetus layers ($I_{\mathrm{fetus}}(d)$) for a given source-detector distance was calculated, by subtracting the signals for the two simulations. By subtracting, we can remove the light and light paths that never made it to the fetus and provide an estimate of what signal is coming from the fetus, albeit, with influences from the mother. $I_{\mathrm{mother}}(d)$ was therefore the photon paths that only traveled through the mother and never through the fetus. $I_{\mathrm{fetus}}(d)$ was the photons that traveled through the mother, reached the fetal layers, travelled back through the mother, ad then detected. As a result, $I_{\mathrm{fetus}}(d)$ also has maternal influences to the signal since the light has to travel through the mother to get to the fetus and then back out again to be detected, but for simplicity, the notation uses the subscript fetus.

Having obtained this difference, the relative contribution of the light passing through the fetus divided by all detected light can be estimated.

$$R_{\mathrm{fetus}}(d) = \frac{I_{\mathrm{fetus}}(d)}{I_{\mathrm{both}}(d)} = \frac{I_{\mathrm{both}}(d) - I_{\mathrm{mother}}(d)}{I_{\mathrm{both}}(d)}, \tag{2}$$

3 | RESULTS

Plots of the MC simulated signal that would be detected at the surface of the mother can be seen in Figure 3. The

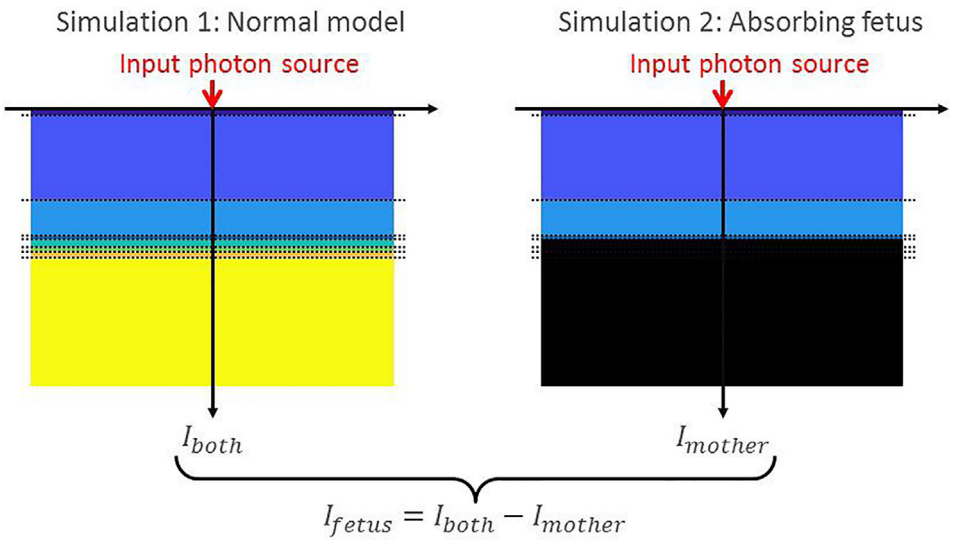

FIGURE 2 Representation of the models for the estimations of light intensity coming from the fetus when there is the normal model (left) and when the fetus layers are set to a very high absorption (right)

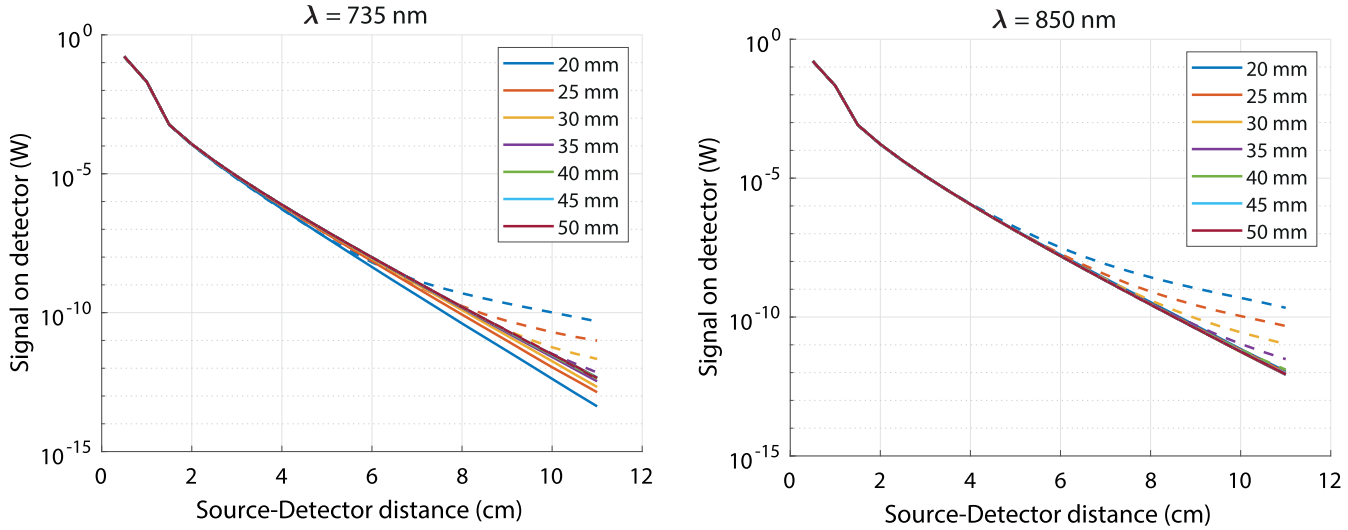

FIGURE 3 Detected power (W) vs the source-detector distance for different wavelengths and fetal depths calculated by Monte Carlo with (dashed lines) and without (solid lines) amniotic fluid, assuming a 200 mW input power and 1 cm^2 detector for 735 nm (left) and 850 nm (right)

source is located at position 0 cm, and therefore, there is greater signal at the shorter source-detector distances. The signal decreases as the source-detector distance increases. This trend was linear (when in log) for the simulations without amniotic fluid, but not for the simulations that have the amniotic fluid layer. For the 735 nm source without amniotic fluid, the 20 mm fetal depth has the greatest decrease in signal compared to 50 mm. The two models with and without amniotic fluid show a clear difference. At the close source-detector distances, the simulations are similar, but then deviate starting around 5 cm depending on fetal depth. Figure 4 shows a close up version of the power levels to better see the difference in the simulations. For example, at the 20 mm fetal depth there was about a two magnitude difference in the signal with and without amniotic fluid at a source-detector distance of 9.5 cm at 735 nm. The shallow depths displayed this larger difference between the two models compared to the deeper depths. At the fetal depth of 35 mm the two models diverge at about 8.5 and 7.5 cm for the 735 and 850 nm sources, respectively. When the fetal depth was 45 mm (Figure 4C,D), there was very little difference between the models with and without amniotic fluid. PHD maps were made from the simulation results for with (Figure 5) and without (Figure 6) amniotic fluid. The figures show the most likely path that the photon packages would travel, usually resulting in a banana shape, but dependent on the location of the various layers. For both models, when the source detector distance was small, the light was more likely to travel in the

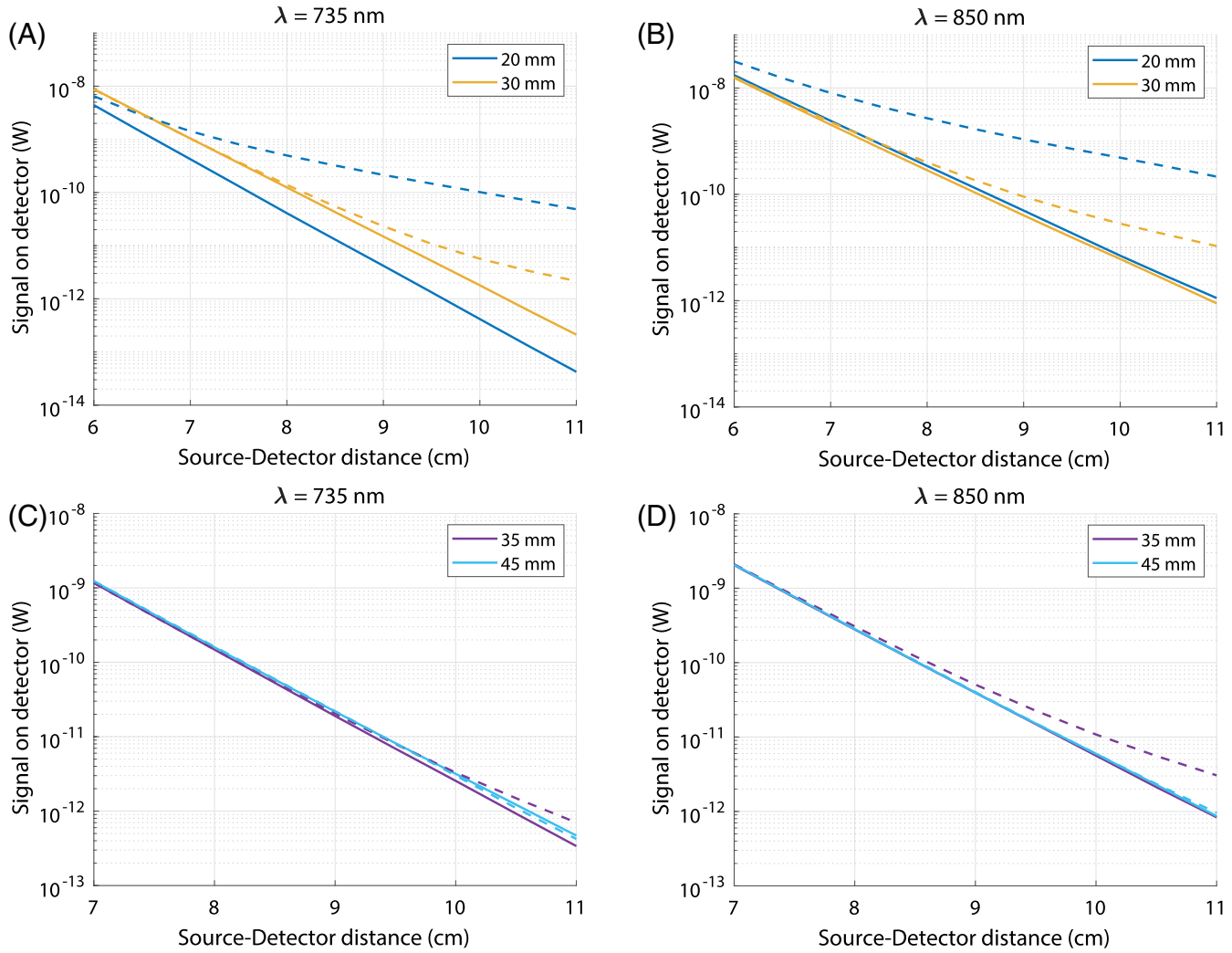

FIGURE 4 Detected power (W) vs the source-detector distance for different wavelengths and fetal depths (20 mm and 30 mm (A,B) and 35 mm and 45 mm (C,D)) calculated by Monte Carlo with (dashed lines) and without (solid lines) amniotic fluid, assuming a 200 mW input power and 1 cm^2 detector for 735 nm (A,C) and 850 nm (B,D)

mother layers. As the source-detector distance increased, the likelihood that the light traveled deeper also increased. When the fetal depth is shallow (20 mm), then the fetal layer is more likely to have light travel through it. However, for deeper fetuses (50 mm), there is unlikely much light that will pass through the fetal layer. There was not any visible difference between PHD maps of the two models, but further analysis shows variation of the two models. Figure 7 shows how the ratio of the sum of the PHD within the fetus over the sum of the PHD of the whole volume. The likelihood of light entering the fetal layer decreases as the fetal depth increases. The larger source-detector distance (95 mm) had a greater likelihood of light that has traveled through the fetal layer will be detected compared to the shorter source-detector distances. The model without amniotic fluid showed a slightly less likelihood than the one with amniotic fluid.

Then the fetal contribution to the signal was determined by subtracting the two models with and without the fetus as discussed in Figure 2. Similar to the total detected signal (Figures 3 and 4), the fetal signal decreases as the source-detector distance increases (Figure 8). Also, as expected, the fetal signal decreases with the fetal depth. The fetal signals from the MC model that were 35 mm and deeper were removed since the MC model lacked the sensitivity to resolve the signal from those depths despite the 1 billion photon packages launched. At the larger depths, the signal was on the order of between 10^{-10} and 10^{-12} W at the larger source-detector distances.

The ratios of the fetal signal ($I_{\text{fetus}}(d)$) over the overall signal were compared in Figure 9A,B. Here, optical signals, not PHD was compared. Some of the MC fetal depths had poor signal to noise ratio (SNR) for the deeper

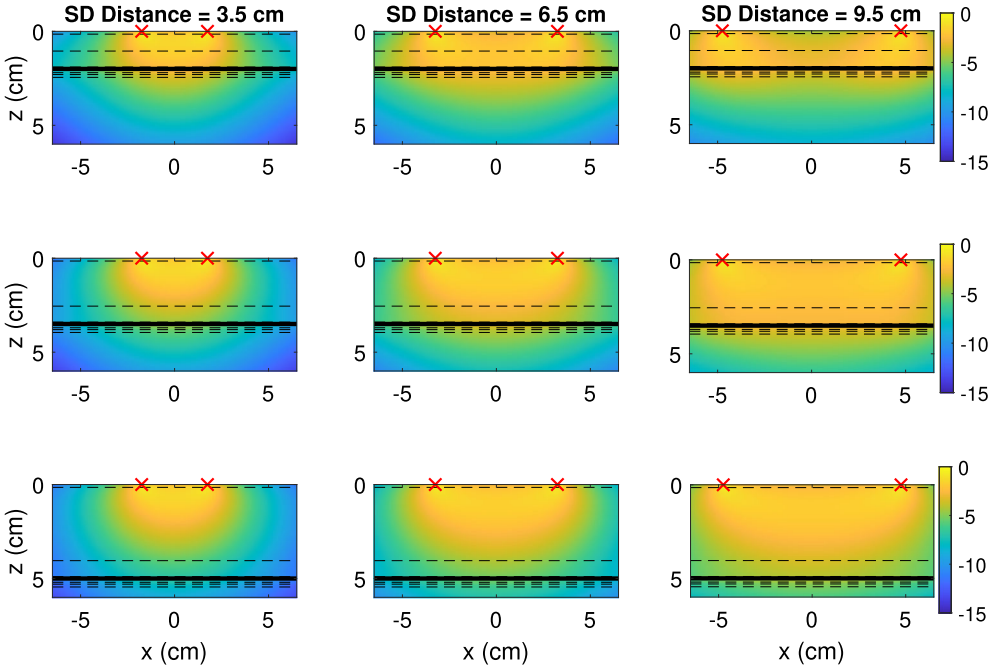

FIGURE 5 Photon hitting density maps from the Monte Carlo simulations with amniotic fluid at 850 nm for three source-detector (SD) distances (3.5, 6.5, and 9.5 cm) and for 20 mm fetal depth (top row), 35 mm fetal depth (middle row), and 50 mm fetal depth (bottom row). The red x's show the location of the source and the detector. The black dotted lines show the interface of each of the layers and the solid black line shows the interface between mother and fetus (see Figure 1).Last, the color represents the density of photons (a.u. in log) in which yellow represents more photons and blue is less. The maps were normalized to the peak value

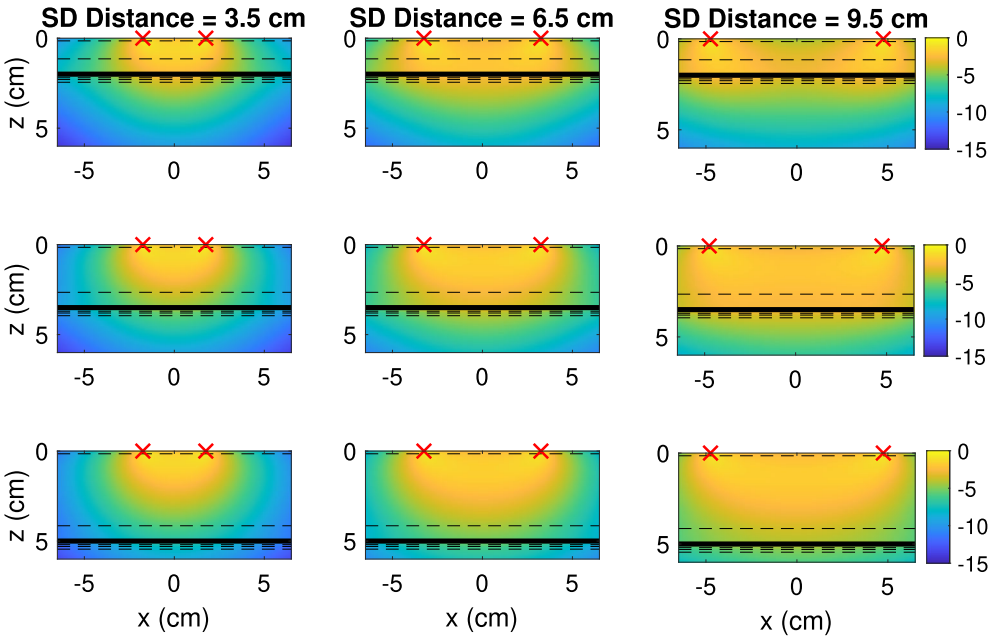

FIGURE 6 Photon hitting density maps from the Monte Carlo simulations without amniotic fluid at 850 nm for three source-detector (SD) distances (3.5, 6.5, and 9.5 cm) and for 20 mm fetal depth (top row), 35 mm fetal depth (middle row), and 50 mm fetal depth (bottom row). The red x's show the location of the source and the detector. The black dotted lines show the interface of each of the layers and the solid black line shows the interface between mother and fetus (see Figure 1). Last, the color represents the density of photons (a.u. in log) in which yellow represents more photons and blue is less. The maps were normalized to the peak value

fetal depths. In general, the ratio for the models are sigmoid in shape and are between zero and one (though never actually reaches one). The deeper the fetal depth the lower the ratio values were with the 20 mm fetal depth showing the greatest ratio values across all source-detector distances. At the shorter source-detector distances, the two models already begin to deviate as the source-detector distance increased. The model without amniotic fluid amniotic fluid generally had lower ratios compared to the model with amniotic fluid for the same fetal depth. A greater portion of the signal comes from the fetus at the larger source-detector distances. For

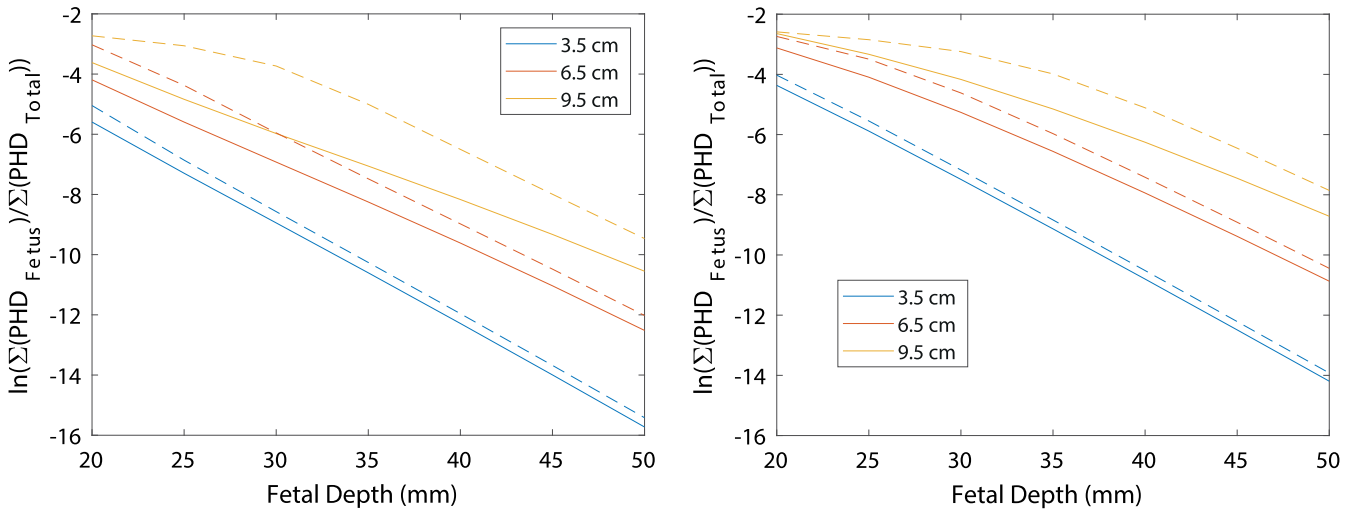

FIGURE 7 The ratio of the photon hitting density within the fetal region over the overall photon hitting density values for Monte Carlo (MC) without amniotic fluid (solid lines) and with amniotic fluid (dashed lines). The ratios were calculated from the photon hitting density (PHD) maps from the MC simulations at 735 nm (left) and 850 nm (right) for three source-detector (SD) distances (3.5, 6.5, and 9.5 cm) and for 20 to 50 mm fetal depths

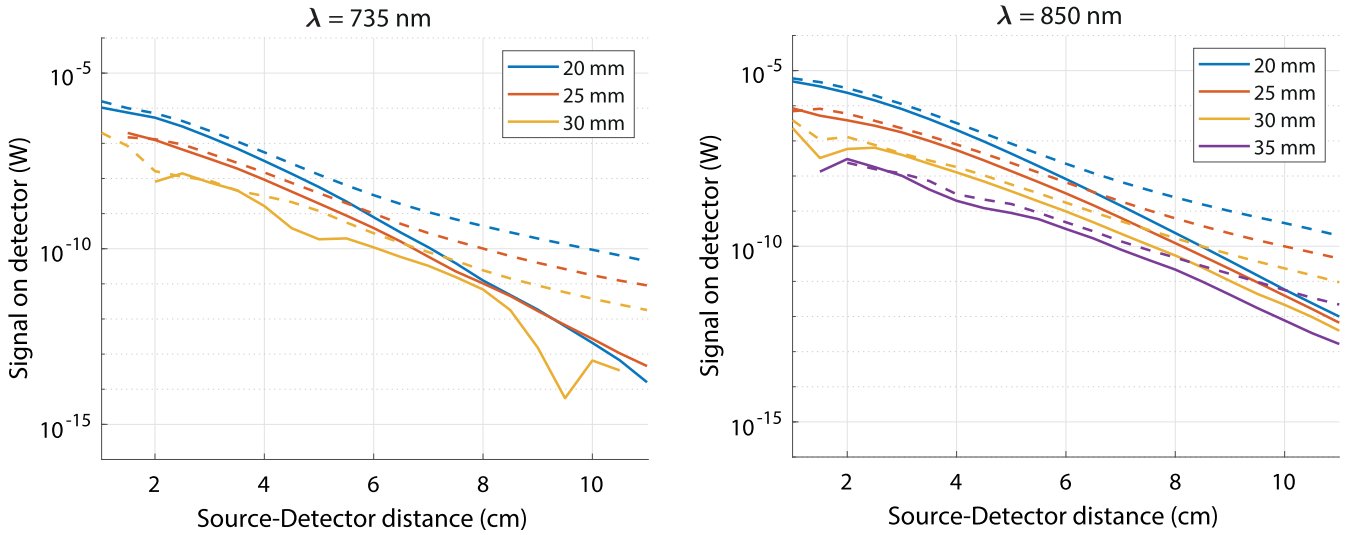

FIGURE 8 The signal on the detector that was attributed to the light that passed through the fetal layers for 735 nm (left) and 850 nm (right) for different fetal depths (legend). The solid lines represent the Monte Carlo (MC) model without amniotic fluid, the dashed lines are the MC simulations with amniotic fluids. Curves for MC simulations of the fetal signal for fetal depths >30 mm were omitted due to poor signal-noise-ratio

example, more than 50% of the signal was from the fetus (with amniotic fluid) if the source was 850 nm and the fetal depth was 25 mm or less when the source-detector distance was greater than about 7 cm.

4 | DISCUSSION

MC simulations were used to be able to study how amniotic fluid affects the signal of transabdominal fetal monitoring. Amniotic fluid has very low scattering properties and does not fall into the diffusion regime, but MC can still simulate low scattering material. The behavior of the signal with and without the presence of amniotic fluid was very different. In some cases (ie, 20 mm) there were several orders of magnitude difference between the two models, with the amniotic fluid model showing greater signal. Here, the amniotic fluid layer was only 1 mm in width, but at the larger source detector distances this layer still influences the signal. However, at the

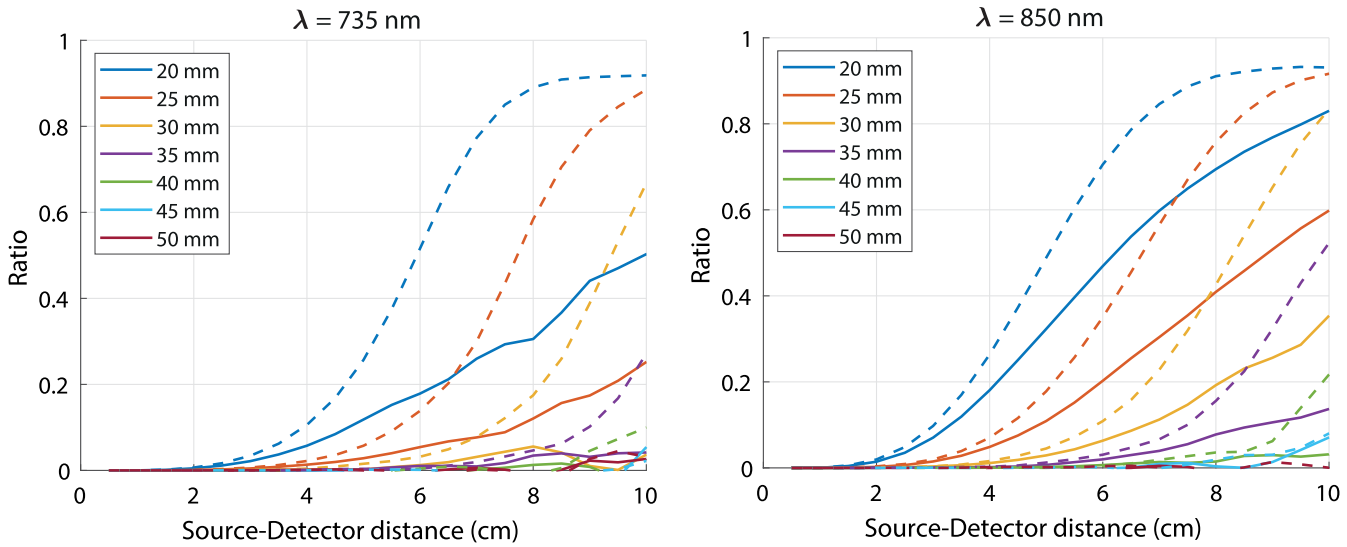

FIGURE 9 The ratio of the fetus over the overall signal at different source-detector distances and fetal depths (legend) for 735 nm (left) and 850 nm (right). The solid lines represent the Monte Carlo model without amniotic fluid, the dashed lines are the MC simulations with amniotic fluids

greater fetal depths the influence of the amniotic fluid layer begins to diminish, which may be simply due to the fact that there was less light getting to the fetus and the amount of amniotic fluid compared to the rest of the mother volume being probed by the light was much smaller. Therefore, the amniotic fluid layer seems to make a larger impact in the signal when the fetus is shallow. The 735 nm signal (Figures 3 and 4) showed that the shallower fetal depths had the lower signals compared to the deeper depths. This could be due to the fact that the mother's optical properties at this wavelength are lower compared to the fetal optical properties. Thus, when the fetus is close to the surface of the mother, more light is absorbed at 735 nm because of the larger absorption coefficient of the fetus. The PHD maps showed the likelihood of where the light will travel for a particular detector location. These maps show that detecting light that reached the fetus as the fetal layer depth increased was less likely and that increasing the source-detector distances will increase the likelihood of light reaching the fetal layers and being detected. There was slightly less chance of light going to the fetus with the non-amniotic fluid model. This might also be due to the fact that the non-amniotic fluid model had 1 mm of tissue added to it in the subdermal maternal layer. The 1 mm was added in order to keep the distance between the surface of the mother and the top of the fetal head the same for both models. This added millimeter was much more absorbing than the amniotic fluid layer and may have resulting in a slight decrease in magnitude in the PHD but also in the signal. However, this was a reasonable substitution to make since the fetal depth must be kept the same in order to compare the models and in real life situations the absolute distance between surface and fetus is the most readily available measurement via ultrasound imaging. While Figure 9 showed that there was a greater ratio as the source-detector distance increases, this need to be balanced with the amount of power that can be detected at the larger distances, which were already explained in Figures 3 and 8. These results were similar to the literature where MC five layer models were simulated with optical properties that were valid between 800 and 900 nm. There was an increase in the ratio and then leveled [9, 10]. The spherical model showed a decrease in the ratio at source-detector distances greater than 8 cm, while the planar model continued to stay level [9]. The ratios for the fetal contributions to the signal show interesting trends. The greater the source-detector distance the more fetal influence in the overall signal. However, at the deeper fetal depths, this signal ratio is greatly reduced. Even at a fetal depth of 35 mm the fetal component was less than 30% for the 735 nm laser source. For system design, obtaining the small fetal contribution at greater depths will be important for the success of a system. This quantifies the optical shunt problem described in Reference [5], where part of the light just travels through the mother, but another part travels through the mother and fetus. Our fraction of light from the fetus (Figure 9) was lower than that of Reference [5] because they used 1 cm mother layer and a 1 cm amniotic layer (our simulations were 1 mm) with very low absorption and scattering coefficients ($\mu_a = 0.012$ cm^{-1} and $\mu_s' = 0.1$ cm^{-1}) for the amniotic fluid. The lower optical properties resulted in more light entering the fetal

layer. The fetal signal in this article (Figure 8) also includes part of this mother signal, which is difficult to separate. The fetal signal will always be mixed with the mother signal since the light must travel through the mother layers in order to be detected. Therefore, obtaining accurate oxygen saturation levels of the fetus alone is difficult [5]. Furthermore, there was a big disparity between the ratios for the models with and without amniotic fluid. For example, for the 735 nm case, there was nearly a 50% difference between the two models at a source-detector distance of 10 cm. The presence of the amniotic fluid actually assists in the light reaching the fetus and being detected at the surface. There might be two reasons for this phenomenon. First, is the 1 mm layer of subdermal maternal compared to 1 mm of amniotic fluid, which has much lower scattering and absorption. However, with other simulations that just remove the amniotic fluid layer and not compensate for fetal depth (data not shown), the results are similar with just a slight increase in magnitude. The other explanation could be due to the low scattering nature of the amniotic fluid. Without the amniotic fluid layer present, the photon could reach the fetus, reflect, and immediately be scattered and absorbed in the mother layers. With the fluid, the chances of reaching the fetus could have increased.

The MC methods used in the current study were inspired by the work of Fong et al. [13] The same optical properties, as well as, similar fetal depths were used. However, there are very key differences and improvements to the methods used in the current study. First, a GPU MC code was used that allowed for simulations with 1 billion photon packages, allowing for greater accuracy at farther source-detector distances and depth of the simulations. When fewer photon packages were run (data not shown), the simulation results were extremely noisy at the larger source-detector distances. The other study [13] used 25 million (340 million for greater depths), which would most likely result in very noisy data at the larger source-detector distances and is unclear how this was avoided. Second, the intensity was integrated over a 1 cm^2 detector area to mimic a possible system. Our ratio results were very similar to the ratios plotted in Reference [13], showing similar trends and a lack of fetal light detected at the greater fetal depths. However, our results for the signal from the fetal layer (Figure 8) are about one to two magnitudes lower due to the source power used. Here, we present results with a source power similar to the limit for laser exposure to skin (200 m W cm^{-2}). Last, there were two simulations done with and without a fetus (high absorption layer) to obtain the fetal influence on the signal. The subtraction methods was taken from Zourabian et al. [5], but there were only three layers in this model, so our model was expanded to the eight layers presented here. These methods can be used on commonly available software without modifications.

Comparison of diffusion and radiative transport models with phantom studies was done by Vishnoi et al. [15] They found that the simulations best matched the phantom results when the fetal head was close to the uterine wall, which would be for near-term pregnancies. Additionally, their models with low absorbing and low scattering amniotic fluid in the photon path did not match the clinical results. This confirms the hypothesis that amniotic fluid plays a role in signal detection and affects light propagation modeling. They also argue that transport theory is necessary when modeling low-absorbing, low-scattering media. MC is also capable of modeling these media, which we present here. Last, Vishnoi et al. suggests that simpler diffusion models can be used at near-term pregnancies because the effect of the amniotic fluid layer is diminished [15]. Our study agrees with these findings. The presence of amniotic fluid, even for a width of 1 mm, impacts the results of the simulations. However, if the fetus is directly placed against the uterus for near-term pregnancies, this effect will decrease. Therefore, for pre-natal screening, models such as MC or radiative transport must be used, but for near-term pregnancies or in labor monitoring, diffuse models may be sufficient.

Overall, the optical signals from a fetus in utero can be recovered given sufficient optical input power, proper detectors with sufficient noise equivalent power (NEP), and fetal depth of no more than about 35 to 40 mm. Using the NEP value of a typical detector ($1.5 \times 10^{-14} \mathrm{W}/\sqrt{\mathrm{Hz}}$) and a reasonable bandwidth of 20 Hz, the fetal component of the signal can be detected. From the simulations, source-detector distance that is recommended is around 6 to 8 cm, since this gave the highest ratio of fetal signal with sufficient detectable power above the NEP level. This source-detector distance range allows for enough signal from the fetal layers, while still providing enough power to be detectable. However, the optimal source-detector distance is dependent on the fetal depth. From the results, the presence of amniotic fluid at the longer source-detector positions aid in this this detection. Moving forward, we will examine the change in the signal due to the heart beat of the fetus. The change in signal due to the pulse is what is needed to yield the actual arterial oxygen content. This adds another layer of challenge but is necessary for developing methods towards fetal monitoring. Here, we determined how much of the light actually reaches the fetus given different source-detector distances and fetal depths. Other future work will consist of adding dynamic signals to both mother and fetus in order to observe how the signal is effected by both heart

beats. Additionally, the thickness of the amniotic fluid layer will most likely have an influence on the signal, and this should be studied as well moving forward. This will help determine the limitations of pre-natal screening using transabdominal fetal monitoring compared to during labor monitoring.

5 | CONCLUSION

The work presented here indicates that it is feasible to recover fetal signals through the abdomen of a pregnant mother in order to perform non-invasive transabdominal fetal pulse oximetry. This is supported by the literature that has revealed several successful studies and the improved modeling from our team using accurate MC simulations (improved algorithm allowing more photon packages; 1 billion). The fetal signal power contribution varies widely depending upon fetal depth and source-detector distance. We present both the mother and fetal contributions to the overall signal, showing more contribution from the fetus at greater source-detector distances. The PHD maps showed the probability of obtaining light in the fetal layer given a particular source-detector distance. Last, we demonstrated a significant difference in the simulations when amniotic fluid was and was not present, especially at longer source-detector distances. Future studies will consist of varying the width of the amniotic fluid layer. Additionally, fetal pulse must be included in the model in order to successfully determine arterial fetal oxygenation.

ACKNOWLEDGMENTS

We would like to thank Dr Neil Ray from Raydiant Inc., and Dr Nevan Hanumara from MIT for their input and discussions. We would like to thank Sunrise labs for their support. We would also like to acknowledge Raydiant Inc. for their financial support to Tyndall National Institute. Additionally, we would like to acknowledge the Science Foundation Ireland (SFI/15/RP/2828 and SFI/12/RC/2276 P2) for the funding provided to Tyndall National Institute. Open access funding provided by IReL.

CONFLICTS OF INTEREST

Jana M. Kainerstorfer is a consultant for Raydiant Inc. and has financial interests in the company. The other authors have no conflicts of interest to disclose.

AUTHOR CONTRIBUTIONS

Jacqueline Gunther performed the MC simulations and its analysis. Baptiste Jayet assisted with the setup and analysis of the data. Adam Jacobs provided relevant information as inputs into the simulations (optical properties, wavelengths, etc.). Ray Burke, Jana M. Kainerstorfer, and Stefan Andersson-Engels supervised the work done and provided input for the analysis.

DATA AVAILABILITY STATEMENT

The data that support the findings of this study are not available due to ongoing industry collaboration.

ORCID

Jacqueline Gunther https://orcid.org/0000-0001-7993-2983

REFERENCES

[1] J. A. Martin, B. E. Hamilton, M. J. K. Osterman, Births: Final Data for 2019 Report National Center for Health Statistics. Division of Vital, Statistics. https://stacks.cdc.gov/view/cdc/100472, **2021**.

[2] World Health Organization, WHO Statement on Caesarean Section Rates, **2015**. https://www.who.int/reproductivehealth/publications/maternal_perinatal_health/cs-statement/en/.

[3] Keila Cristina Mascarello, Bernardo Lessa Horta, Mariângela Freitas Silveira, *Revista de saude publica* **2017**, *51*, 105.

[4] T. J. Garite, G. A. Dildy, H. McNamara, M. P. Nageotte, F. H. Boehm, E. H. Dellinger, R. A. Knuppel, R. P. Porreco, H. S. Miller, S. Sunderji, *Am. J. Obstet. Gynecol.* **2000**, *183*(5), 1049.

[5] A. Zourabian, A. M. Siegel, B. Chance, N. Ramanujam, M. E. Rode, D. A. Boas, *J. Biomed. Opt.* **2000**, *5*(4), 391.

[6] K. B. Gan, E. Zahedi, M. A. M. Ali, *Optica Applicata* **2011**, *41*(4), 885.

[7] N. Ramanujam, G. Vishnoi, A. H. Hielscher, M. E. Rode, I. Forouzan, B. Chance, *J. Biomed. Opt.* **2000**, *5*(2), 173.

[8] S. Ley, D. Laqua, P. Husar, *The 15th International Conference on Biomedical Engineering*, Springer, Cham **2014**, p. 356.

[9] M. Bottrich, S. Ley, P. Husar, *Curr. Dir. Biomed. Eng.* **2015**, *1*(1), 450.

[10] Marcel Bottrich, Sebastian Ley, Peter Husar, Engineering in Medicine and Biology Society (EMBC), 2015 37th Annual Int. Conf. IEEE, pp. 5122–5125.

[11] Marcel Bottrich, in 2018 40th Annual International Conference of the IEEE Engineering in Medicine and Biology Society (EMBC), IEEE, pp. 5870–5873.

[12] L. Steven, N. R. Jacques, G. Vishnoi, R.-G. Choe, B. Chance, *J. Biomed. Opt.* **2000**, *5*(3), 277.

[13] Daniel Fong, André Knoesen, Soheil Ghiasi, in 2017 IEEE 19th Int. Conf., IEEE, pp. 1–6.

[14] D. Paul, J. R. C. Mannheimer, M. E. Fein, S. L. Nierlich, *IEEE Trans. Biomed. Eng.* **1997**, *44*(3), 148.

[15] G. Vishnoi, A. H. Hielscher, N. Ramanujam, B. Chance, *J. Biomed. Opt.* **2000**, *5*(2), 163.

[16] Stefan Borik, Ivona Malikova, Johannes Miersch, Daniel Laqua, Sebastian Ley, Peter Husar, in ELEKTRO, 2014, IEEE, pp. 526–530.

[17] Daniel Laqua, Stefan Pollnow, Jan Fischer, Sebastian Ley, Peter Husar, in Engineering in Medicine and Biology Society (EMBC), 2014 36th Annual Int. Conf. IEEE, pp. 5631–5634.

[18] D. Laqua, C. Brieskorn, J. H. Koch, M. Rothmayer, S. Zeiske, M. Böttrich, P. Husar, *Curr. Dir. Biomed. Eng.* **2016**, *2*(1), 689.

[19] D. Daniel, A. K. Fong, M. Motamedi, T. O'Neill, S. Ghiasi, *Smart Health* **2018**, *9*, 23.
[20] T. Uchida, N. Kanayama, K. Kawai, M. Niwayama, *J. Biomed. Opt.* **2016**, *21*(4), 040502.
[21] S. Nioka, M. Izzetoglu, T. Mawn, M. J. Nijland, D. Boas, B. Chance, *J. Matern. Fetal Neonatal Med.* **2005**, *17*(6), 393.
[22] K. Hiwatashi, K. Doi, R. Mizuno, M. Yokosuka, *J. Biomed. Opt.* **2017**, *22*(2), 026006.
[23] R. Choe, T. Durduran, G. Yu, M. J. M. Nijland, B. Chance, A. G. Yodh, N. Ramanujam, *Proc. Natl. Acad. Sci.* **2003**, *100* (22), 12950.
[24] N. Ramanujam, H. Long, M. Rode, I. Forouzan, M. Morgan, B. Chance, *J. Maternal-Fetal Med.* **1999**, *8*(6), 275.
[25] M. Anthony, S. N. Vintzileos, M. Lake, P. Li, Q. Luo, B. Chance, *Am. J. Obstet. Gynecol.* **2005**, *192*(1), 129.
[26] K. B. Gan, E. Zahedi, M. A. M. Ali, *IEEE Trans. Biomed. Eng.* **2009**, *56*(8), 2075.
[27] T. Uchida, N. Kanayama, M. Mukai, N. Furuta, H. Itoh, H. Suzuki, M. Niwayama, *J. Perinat. Med.* **2016**, *44*(7), 745.
[28] T. Uchida, N. Kanayama, K. Kawai, M. Mukai, K. Suzuki, H. Itoh, M. Niwayama, *J. Obstet. Gynaecol. Res.* **2018**, *44*, 2127.
[29] J. Gunther, B. Jayet, R. Burke, S. Andersson-Engels, *European Conference on Biomedical Optics*, Optical Society of America, Washington DC **2019**, 11074_31.
[30] Erik Alerstam, Tomas Svensson, Stefan Andersson-Engels, *J. Biomed. Opt.* **2008**, *13* (6), 060504.
[31] L. Wang, S. L. Jacques, L. Zheng, *Comput. Methods Programs Biomed.* **1995**, *47*(2), 131.
[32] ANSI Standard, Inc., New York **1993**.
[33] M. Firbank, M. Hiraoka, M. Essenpreis, D. T. Delpy, *Phys. Med. Biol.* **1993**, *38*(4), 503.
[34] S. L. Jacques, *Phys. Med. Biol.* **2013**, *58*(11), R37.
[35] L. Wang, S. L. Jacques, L. Zheng, *Comput. Methods Programs Biomed.* **1997**, *54*(3), 141.

How to cite this article: J. Gunther, B. Jayet, A. Jacobs, R. Burke, J. M. Kainerstorfer, S. Andersson-Engels, *J. Biophotonics* **2021**, e202000486. https://doi.org/10.1002/jbio.202000486